Brillouin light scattering from quantized spin waves in micron-size magnetic wires

J. Jorzick, S. O. Demokritov, C. Mathieu, and B. Hillebrands
Fachbereich Physik und Schwerpunkt Materialwissenschaften, Universität Kaiserslautern, 67653 Kaiserslautern, Germany

B. Bartenlian and C. Chappert
IEF, Université Paris Sud, 91405 Orsay, France

F. Rousseaux
Laboratoire de Microstructures et Microélectronique, 92225 Bagneux, France

A. N. Slavin
Department of Physics, Oakland University, Rochester, Michigan 48309
(Received 22 July 1999)

An experimental study of spin-wave quantization in arrays of micron-size magnetic $Ni_{80}Fe_{20}$ wires by means of Brillouin light-scattering spectroscopy is reported. Dipolar-dominated Damon-Eshbach spin-wave modes laterally quantized in a single wire with quantized wave vector values determined by the width of the wire are studied. The frequency splitting between quantized modes, which decreases with increasing mode number, depends on the wire sizes and is up to 1.5 GHz. The transferred wave vector interval, where each mode is observed, is calculated using a light-scattering theory for confined geometries. The frequencies of the modes are calculated, taking into account finite-size effects. The results of the calculations are in a good agreement with the experimental data. [S0163-1829(99)00246-5]

I. INTRODUCTION

Miniaturization of magnetic storage devices and sensors causes an increasing interest into patterned magnetic films. Progress achieved in lithographic techniques during the last decade allows the fabrication of high quality, well-controlled laterally defined magnetic structures, like, e.g., dots and wires, of micron or submicron sizes. Although static properties of micron-size magnetic dots and wires have been studied to some extent,[1–4] their high-frequency dynamic properties have been rarely investigated.[5,6] The study of spin waves is a powerful method for probing the dynamic properties of magnetic media in general and those of laterally patterned magnetic structures in particular. From spin-wave measurements basic information on the magnetic properties, such as magnetic anisotropy contributions, the homogeneity of the internal field, as well as coupling between magnetic islands, can be extracted. This information is often hard to obtain with other methods. In addition, dynamic excitations define the time scale of a magnetization reversal process, and therefore they are of fundamental importance to achieve an understanding of the time structure of the reversal. When the size of the object becomes comparable to the wavelength of a spin wave under investigation, quantization (or confinement) effects appear, which lead to dramatic changes in the spin-wave spectrum and the spin-wave density of states. The spin-wave quantization in magnetic wires differs from that in magnetic dots, since the former addresses the quantization of one component of the in-plane wave vector (perpendicular to the wire axis), whereas the latter the quantization of both components. If, moreover, the magnetic field is applied along the wire axis, the static demagnetization field is negligible. This makes the analysis even more straightforward. Therefore the understanding of spin-wave quantization in magnetic wires is a first important step in the investigation of spin-wave quantization in more complex geometries.

II. SPIN-WAVE SPECTRUM OF MAGNETIC WIRES

The problem of the calculation of a spin-wave spectrum for an axially magnetized infinite ferromagnetic wire with a rectangular cross section has never been solved analytically (see, e.g., comments in Ref. 7). However, in a particular case of a thin wire $d \ll w$, where d is the thickness of the wire and w is its width, the spectrum of long-wave magnetic excitations can be calculated approximately using the theory of dipole-exchange spin waves in a magnetic film.[8]

The dipole-exchange spin-wave spectrum in an unlimited ferromagnetic medium is given by the Herring-Kittel formula[9]

$$\nu = \frac{\gamma}{2\pi}\left[\left(H + \frac{2A}{M_S}q^2\right)\left(H + \frac{2A}{M_S}q^2 + 4\pi M_S \sin^2\theta_q\right)\right]^{1/2}, \tag{1}$$

where γ is the gyromagnetic ratio, A is the exchange stiffness constant, $\mathbf{H}$ and $\mathbf{M}_S$ are the applied magnetic field and the saturation magnetization both aligned along the z axis, $\mathbf{q}$ is the three-dimensional wave vector, θ_q is the angle between the direction of the wave vector and the magnetization.

In a magnetic film with a finite thickness d the spin-wave spectrum is modified due to the fact that the translational invariance of an unlimited medium is broken in the vicinity of the film surfaces. An approximate expression for spin-wave frequencies of a film can be written in the form, analogous to Eq. (1) [see Eq. (45) in Ref. 8]:

 ©1999 The American Physical Society

$$\nu=\frac{\gamma}{2\pi}\left[\left(H+\frac{2A}{M_S}q^2\right)\left(H+\frac{2A}{M_S}q^2+4\pi M_S\cdot F_{pp}(q_\parallel d)\right)\right]^{1/2}, \tag{2}$$

where

$$q^2=q_y^2+q_z^2+\left(\frac{p\pi}{d}\right)^2=q_\parallel^2+\left(\frac{p\pi}{d}\right)^2 \tag{3}$$

with the normal to the film surface points along the x direction. $q_\parallel$ is the continuously varying in-plane wave vector, $F_{pp}(q_\parallel,d)$ is the matrix element of the magnetic dipole interaction, and $p=0,1,2,\ldots$ is a quantization number for the so-called perpendicular standing spin waves. Equation (3) is obtained for the dynamic part $\mathbf{m}$ of the magnetization under boundary conditions of ''unpinned'' spins on the film surfaces:

$$\left.\frac{\partial\mathbf{m}}{\partial x}\right|_{x=\pm d/2}=0. \tag{4}$$

For the description of the spin-wave modes in our permalloy samples one can use the above boundary condition instead of the general one:[10]

$$\pm\frac{\partial\mathbf{m}}{\partial y}+D\mathbf{m}|_{y=\pm w/2}=0 \tag{4a}$$

with the ''pinning'' parameter D determined by the effective surface anisotropy k_S and the exchange stiffness constant A: $D=k_S/A$. The approximation $D=0$ is justified by the small values of anisotropies in permalloy.

In the case when the spin wave is propagating in the film plane, but perpendicular to the bias magnetic field ($q_z=0$, $q_\parallel=q_y$,) the expression for the matrix element of the dipole-dipole interaction $F_{pp}(q_\parallel d)$ has the form[8]

$$F_{pp}=1+\frac{4\pi M_s}{H+(2A/M_s)q^2}P_{pp}(1-P_{pp}), \tag{5}$$

where the function $P_{pp}(q_\parallel,d)$ for the lowest thickness mode ($p=0$) is given by[8]

$$P_{00}=1-\frac{1-\exp(-q_\parallel d)}{q_\parallel d}. \tag{6}$$

The explicit expressions for P_{pp} when $p>0$ are also given in Ref. 8 [see Eq. (A12) in Ref. 8].

In a long-wavelength ($q_\parallel\cdot d<1$) neglecting exchange ($A=0$) the dispersion equation for the lowest thickness mode ($p=0$) obtained from Eqs. (2), (5), and (6) gives the results that are very similar to the results obtained from the Damon-Eshbach (DE) formula:[11]

$$\nu_{\mathrm{DE}}=\frac{\gamma}{2\pi}\cdot[H\cdot(H+4\pi M_s)+(2\pi M_s)^2\cdot(1-e^{-2q_\parallel d})]^{1/2}. \tag{7}$$

Thus if the film is magnetized in plane and $\mathbf{q}_\parallel\perp\mathbf{M}_s$, the spin-wave modes described by Eqs. (2)–(6) can be divided into the dipole dominated surface mode ($p=0$) and exchange dominated, thickness or perpendicular standing spin-wave (PSSW) modes ($p>0$). The frequency of the former is determined by either Eq. (2) (with $p=0$) or Eq. (7), while the frequencies of the perpendicular standing modes ($p>0$) can be approximately calculated from the expression

$$\nu_p=\frac{\gamma}{2\pi}\left(\left[H+\frac{2A}{M_S}q_\parallel^2+\frac{2A}{M_S}\left(\frac{p\pi}{d}\right)^2\right]\times\left\{H+\left[\frac{2A}{M_S}+H\left(\frac{4\pi M_s/H}{p\pi/d}\right)^2\right]q_\parallel^2+\frac{2A}{M_S}\left(\frac{p\pi}{d}\right)^2+4\pi M_S\right\}\right)^{1/2} \tag{8}$$

which is obtained from Eq. (2) in the limit $q_\parallel d\ll 1$ using the expressions for the dipole-dipole matrix elements $F_{pp}(q_\parallel d)$ calculated in Ref. 8. It is clear from Eq. (8) that the $\nu_p(q_\parallel)$ dependence is rather weak for $q_\parallel\ll p\pi/d$. In the general case $q_\parallel d>1$ numerical approach is usually used for the determination of the spin-wave frequencies in films.[12]

Equations (2)–(8) provide a proper description of the spin-wave frequencies apart from the intervals of mode crossing ($\nu_0\approx\nu_p$) where an essential mode hybridization takes place. In these regions numerical calculations are also necessary to obtain the correct spin-wave spectrum of the film.[8,12]

If we consider a magnetic wire magnetized in plane along the z direction and having a finite width w along the y direction as shown in Fig. 1, a boundary condition similar to Eq. (4) at the lateral edges of the wire should be imposed:

$$\left.\frac{\partial\mathbf{m}}{\partial y}\right|_{y=\pm w/2}=0. \tag{9}$$

An additional quantization of the y component of $\mathbf{q}_\parallel$ is then obtained:

$$q_{y,n}=\frac{n\pi}{w}, \tag{10}$$

where $n=0,1,2,\ldots$. Using Eqs. (2), (7), and (8) and the quantization expression (10) one can calculate the frequencies of width (or laterally quantized) modes. The profile of the dynamic part of the magnetization $\mathbf{m}$ in the nth mode can be written as follows:

$$\mathbf{m}_n(y)=\mathbf{a}_n\cdot\cos\left[q_{y,n}\left(y+\frac{w}{2}\right)\right],\quad -\frac{w}{2}<y<\frac{w}{2}. \tag{11}$$

Equation (11) describes a standing mode consisting of two counterpropagating waves with quantized wave vectors $q_{y,n}$. Note here that due to the truncation of the cos function at the wire boundaries, the quantized values $q_{x,p}$ and $q_{y,n}$ are not true wave vectors.

Calculations of the quantized dipole dominated surface modes in an axially magnetized elliptical cylinder have been performed by DeWames and Wolfram.[13] They showed that all modes can be characterized by a positive integer and the wave vector component along the axis of the cylinder q_z. The calculated surface mode frequencies are closely related to the DE modes of an infinite film. For $q_z\neq 0$ no simple quantization scheme can be used, because a quantization parameter cannot be defined independent of q_z. However, when $q_z=0$, these modes correspond to DE modes with quantized in-plane wave vector. Since the magnetic wires

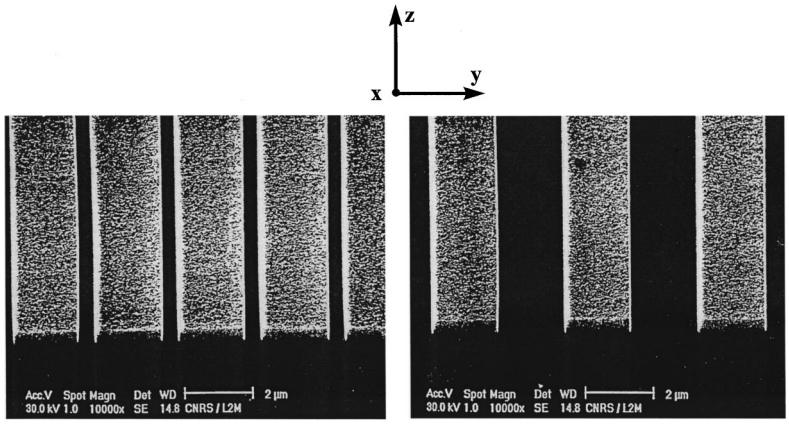

FIG. 1. Scanning electron micrographs of the permalloy wires under investigation. The orientation of the Cartesian coordinate system used for calculations is shown as well.

investigated in the present work are not ellipsoidal, having a rectangular cross section, the quantitative results as obtained in Ref. 13 cannot be used directly. Nevertheless, they are very useful for a qualitative understanding.

III. BRILLOUIN LIGHT SCATTERING ON MAGNETIC WIRES

Brillouin light scattering (BLS) has been used since a long time ago for the investigation of spin waves in thin magnetic films and layered structures.[14,15] However, this technique is particularly well suited for the investigation of spin waves in laterally patterned systems. The main advantages of BLS are a high spatial resolution defined by the size of the laser beam focus, which is 30–50 μm in diameter, and the possibility to investigate spin waves with different absolute values and orientations of their wave vectors. The former circumstance allows one to investigate small pattern areas, which simplifies the patterning procedure. The latter provides information on the lateral distribution of the dynamic component of the magnetization in a laterally confined island.

The Brillouin light-scattering process can be considered as a creation (absorption) of a magnon by a photon. In the case of magnon absorption the photon increases its energy and momentum:

$$\hbar\omega_S=\hbar(\omega_I+\omega),$$
$$\hbar\mathbf{q}_S=\hbar(\mathbf{q}_I+\mathbf{q}) \tag{12}$$

where $\hbar\omega_I$, $\hbar\omega_S$, $\hbar\omega$ and $\hbar\mathbf{q}_I$, $\hbar\mathbf{q}_S$, $\hbar\mathbf{q}$ are the energy and the momentum of the incident and scattered photons and of the absorbed magnon, correspondingly. From Eq. (12) it is evident that the wave vector $\mathbf{q}_S-\mathbf{q}_I$, transferred in the scattering process, is equal to $\mathbf{q}$. To understand this fact one should consider the differential light-scattering cross section $d^2\sigma/d\Omega d\omega_S$, i.e., the number of photons scattered into the solid angle $d\Omega$ in the frequency interval between ω_S and $\omega_S+d\omega_S$ per unit incident flux density, which can be written as follows:[16]

$$\frac{d^2\sigma}{d\Omega\, d\omega_S}\propto\langle\delta\varepsilon^*(\mathbf{q}_I-\mathbf{q}_S)\,\delta\varepsilon(\mathbf{q}_I-\mathbf{q}_S)\rangle_{\omega_I-\omega_S} \tag{13}$$

with $\delta\varepsilon$ the dynamic (fluctuating) term of the permittivity, which is caused by the spin waves due to magneto-optical effects[17] and which gives rise to the scattering. $\delta\varepsilon$ is proportional to the dynamic part of the magnetization $\mathbf{m}$ of the spin wave. The correlation function in the bracket is given by

$$\begin{aligned}\langle\delta\varepsilon^*(\mathbf{q})\,\delta\varepsilon(\mathbf{q})\rangle_\omega&=\int d(t_2-t_1)d^3(\mathbf{r}_2-\mathbf{r}_1)\\&\quad\times\exp[-i\omega t-i\mathbf{q}(\mathbf{r}_2-\mathbf{r}_1)]\\&\quad\times\langle\delta\varepsilon^*(\mathbf{r}_1,t_1)\,\delta\varepsilon(\mathbf{r}_2,t_2)\rangle\\&\propto\int d(t_2-t_1)d^3(\mathbf{r}_2-\mathbf{r}_1)\\&\quad\times\exp[-i\omega t-i\mathbf{q}(\mathbf{r}_2-\mathbf{r}_1)]\\&\quad\times\langle\mathbf{m}^*(\mathbf{r}_1,t_1)\mathbf{m}(\mathbf{r}_2,t_2)\rangle\end{aligned} \tag{14}$$

with $\langle\cdots\rangle$ the statistical average. If light is scattered from a spin wave propagating in an infinite medium, the spatial integration volume is the entire space. In this case the correlation function in Eq. (12) is nonzero only if the relations $\omega=\omega_S-\omega_I$ and $\mathbf{q}=\mathbf{q}_S-\mathbf{q}_I$ are fulfilled, yielding the conservation laws of energy and momentum, described by Eq. (12). However, since for a spin-wave mode propagating in a film the integration volume is bounded by the two film surfaces, the conservation conditions are fulfilled only for the two in-plane components of the wave vector $\mathbf{q}_\parallel$. In backscattering geometry, when $\mathbf{q}_S=-\mathbf{q}_I$, $q_\parallel$ is determined by the angle of incidence of the light θ: $q_\parallel=2q_I\sin\theta$. The third component perpendicular to the film q_n is not well defined by the conservation law because the system does not possess the symmetry of translational invariance perpendicular to the film. The uncertainty in q_n is, apparently, inversely proportional to t, the thickness of the film or of the mode localization region, or the penetration depth of the light. It is negligible, if $(\mathbf{q}_S-\mathbf{q}_I)_n t\gg 2\pi$.

Since a long magnetic wire possesses *in-plane* translational invariance only along its axis, the in-plane wave vector $\mathbf{q}_\parallel$ is no longer fully conserved in the light-scattering process. The only conserved component is the component of $\mathbf{q}_\parallel$ along the wire axis. It is clear from Eq. (14) that the dependence of the differential light-scattering cross section on the component of $\mathbf{q}_\parallel$ perpendicular to the wires is determined by the Fourier component $\mathbf{m}_{q_\parallel}$ of $\mathbf{m}(\mathbf{r}_\parallel)$:

$$I(q_\parallel)\propto\frac{d^2\sigma}{d\Omega\, d\omega_S}\propto\langle\delta\varepsilon^*(q_\parallel)\,\delta\varepsilon(q_\parallel)\rangle\propto|\mathbf{m}_{q_\parallel}|^2. \tag{15}$$

Thus performing the BLS experiment with different $\mathbf{q}_{\parallel}$ one can obtain the information of the spatial distribution of the magnetization $\mathbf{m}$ in the wire and one can identify the spin-wave mode unambiguously.

As was already mentioned, there are very few studies of the dynamic properties of magnetic wires. In early investigations of BLS from spin waves in an array of permalloy wires Gurney *et al.*[18] have observed a splitting of the spin-wave spectrum into several discrete modes. However, the authors were not able to identify the nature of the modes. Very recently Mathieu *et al.*[19] investigated spin wave in arrays of permalloy wires by BLS. In addition to demagnetization effects a quantization of the spin-wave mode in several dispersionless modes, caused by a confinement effect of the spin waves, was observed and quantitatively described.[19]

IV. EXPERIMENTAL PROCEDURE

The arrays of wires were made of $d=20$- and 40-nm-thick permalloy ($Ni_{80}Fe_{20}$) films. The films were grown by means of *e*-beam evaporation in an UHV-evaporation system (5×10^{-10} mbars base pressure) onto chemically cleaned SiO_2/Si(111) substrates. Patterning was performed using x-ray lithography. The patterning masks were fabricated by means of a JEOL 5D2U nanopattern generator at 50 keV. X-ray exposure was performed at the super-ACO facility (LURE, Orsay, France) using a negative resist and a liftoff process with Al coating and ion milling.[20] In this way two types of samples with a wire width w of 1.8 μm and distances between the wires of 0.7 and 2.2 μm were prepared. The length of the wires l was 500 μm; they were arranged in an array with the entire patterned area of $500\times500\,\mu\mathrm{m}^2$. Thus the aspect ratios of the investigated wires are very high: $l/w=220$, $w/d=45$ or 90. Figure 1 presents a scanning electron microscope image of two arrays of magnetic wires with the same wire widths but with different distances between the wires. As it is clear from Fig. 1, the used technique guarantees a high quality patterning process, which provides a superb flatness of the wire boundaries and reproducibility of the wire widths. An investigation of the magnetization reversal behavior of the structures, performed by Kerr magnetometry, showed that the magnetic easy axis of the array was along the wire axis, which is expected from magnetic shape anisotropy considerations. The demagnetization factors of the wires were determined from hard-axis magnetization curves.

The spin-wave properties were investigated at room temperature by means of BLS in a backscattering geometry using a computer controlled tandem Fabry-Perot interferometer which is described elsewhere.[21,22] Laser light of a single moded, frequency stabilized ($\Delta\nu=20$ MHz) Ar^+ laser with a wavelength of $\lambda_{\mathrm{laser}}=514.5$ nm and a laser power of 50 mW was focused onto the sample and the frequency spectrum of the backscattered light was analyzed. An external field was applied along the wires, while the in-plane wave vector $\mathbf{q}_{\parallel}=(\mathbf{q}_S-\mathbf{q}_I)_{\parallel}$, transferred in the light-scattering process, was oriented perpendicular to the wires, and its value was varied by changing the angle of light incidence θ measured from the surface normal: $q_{\parallel}=(4\pi/\lambda_{\mathrm{laser}})\cdot\sin\theta$. The collection angle of the scattered light was chosen small enough to ensure a reasonable resolution in $q_{\parallel}$ of $\Delta q_{\parallel}=\pm0.8\times10^4$ cm^{-1}. It was shown in test experiments with a better resolution ($\Delta q_{\parallel}/3$), that the collection angle was chosen small enough for the studies presented below. At small angles of light incidence the directly reflected beam and diffraction reflexes entering the collection lens were blocked by small blinds inserted into the collection aperture.

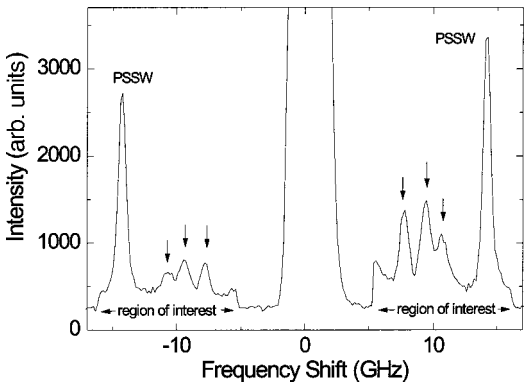

FIG. 2. Experimental Brillouin light-scattering spectra obtained from the sample with a thickness of 40 nm, a wire width of 1.8 μm, and separation of the wires of 0.7 μm. The applied field was 500 Oe orientated along the wire axis and the incoming wave vector of the light was orientated perpendicular to the wires. The transferred wave vector was $q_{\parallel}=0.3\times10^5$ cm^{-1}. In the region of interest (5–17 GHz) the scanning speed was reduced by a factor of 3 increasing the number of recorded photons by the same factor.

Due to possible variation in the transmission of the interferometer during the course of measurements, it is, in general, very difficult to measure absolute values of the BLS scattering cross section. To overcome this problem, we used the PSSW mode, registered for the entire investigated range of $q_{\parallel}$, as a reference for relative measurements of the BLS scattering cross section. The BLS intensity corresponding to each in-plane mode was normalized to the intensity of the PSSW mode. The relative intensities obtained in this way were very reproducible and were used for measuring the lateral distribution of the dynamic magnetization through the wire using the approach discussed above.

V. RESULTS AND DISCUSSION

Figure 2 shows a typical BLS spectrum for the sample with a wire width of 1.8 μm and a separation between the wires of 0.7 μm. A transferred wave vector $q_{\parallel}=0.3\times10^5$ cm^{-1} was oriented perpendicular to the wires, while an external field of 500 Oe was applied along the wire axis. As it is seen in Fig. 2, the spectrum contains four distinct modes near 7.8, 9.3, 10.4, and 14.0 GHz. Note here that in the region of interest (5–17 GHz) the scanning speed of the interferometer was reduced by a factor of 3 to increase the accumulation time in this region and thus to improve the signal-to-noise ratio. By varying the applied field the spin-wave frequency for each mode was measured as a function of the field, as displayed in Fig. 3. The observed dependence of all frequencies on the field confirms that all detected modes are magnetic excitations.

To identify the nature of the observed modes, the dispersion of the modes was obtained by varying the angle of light incidence θ and thus the magnitude of the transferred wave

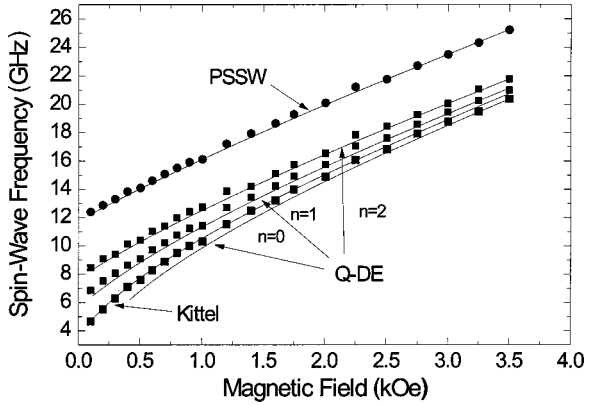

FIG. 3. Frequencies (for $q_{\parallel}=0.3\times10^{5}$ cm^{-1}) of the in-plane quantized spin-wave modes of the wire array with a wire width of 1.8 μm and a wire thickness 40 nm as a function of the applied field. The lines are calculated using either the DE equation with quantized wave vectors (Q-DE) or the Kittel formula [Eq. (17)] as indicated. The line labeled PSSW shows the frequency of the first perpendicular standing spin wave calculated using a numerical procedure (Ref. 12).

vector $q_{\parallel}$. The results are displayed in Fig. 4 for two samples with the same wire thickness of 40 nm and width of 1.8 μm, but with different wire separations of 0.7 μm (open symbols) and 2.2 μm (solid symbols). The dispersion measured on the arrays with the same lateral layout but with a wire width of 20 nm is presented in Fig. 5. It is clear from Fig. 4 that one of the detected modes presented by circles (near 14 GHz) is the PSSW mode, corresponding to $p=1$ in Eq. (8) (it is not seen in Fig. 5 due to its much higher frequency caused by the smaller wire thickness). In the region of low wave vectors the spin-wave modes show a disintegration of the continuous dispersion of the Damon-Eshbach mode of an infinite film into several discrete, resonancelike modes with a frequency spacing between the lowest lying modes of approximately 0.9 GHz for $d=20$ nm and 1.5 GHz for $d=40$ nm. As it is clear from Figs. 4 and 5, there is no significant difference between the data for the wires with a separation of 0.7 and 2.2 μm. This fact indicates that the mode splitting is purely caused by the quantization of the spin waves in a single wire due to its finite width.

As it is seen in Fig. 4, the first PSSW mode ($p=1$) was observed in the arrays with a wire thickness of 40 nm for the entire investigated range of $q_{\parallel}$. It was used as a reference for relative measurements of the BLS scattering cross section, as it was described above. The results of these measurements are shown by black squares in Fig. 6.

Having a closer look at the dispersion curves and the BLS cross section profiles of the magnetic wires one can summarize the main features as follows: (i) For low wave vector values ($0-0.8\times10^{5}$ cm^{-1}) the discrete modes do not show any noticeable dispersion, behaving like standing wave resonances. (ii) Every discrete mode is observed over a continuous range of the transferred wave vector $q_{\parallel}$. (iii) The lowest two modes appear very close to zero wave vector, the higher modes appear at higher values. (iv) The frequency splitting between two neighboring modes is decreasing for increasing mode number. (v) There is a transition regime ($q_{\parallel}=0.8-1.0\times10^{5}$ cm^{-1}) where the well resolved dispersionless modes converge towards the dispersion of the continuous film (see dashed lines in Figs. 4 and 5). (vi) There is no noticeable difference for the samples with the same wire width w but different wire separations (0.7 and 2.2 μm).

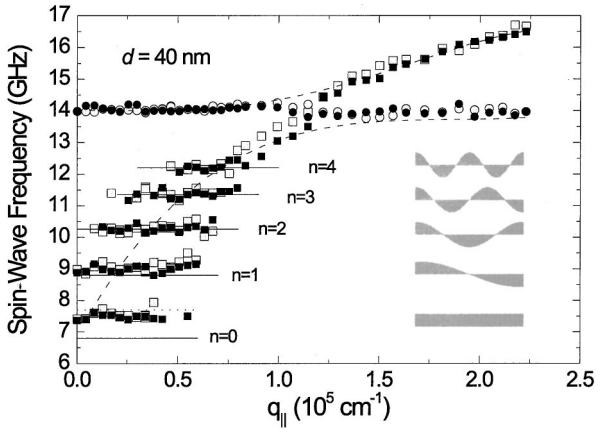

FIG. 4. Obtained spin-wave dispersion curves for an array of wires with a wire thickness of 40 nm, a wire width of 1.8 μm, and a separation between the wires of 0.7 μm (open symbols) and 2.2 μm (solid symbols). The external field applied along the wires axis was 500 Oe. The solid horizontal lines indicate the results of a calculation using Eq. (7) with the quantized values of $q_{\parallel}$. The dotted horizontal line indicates the result of calculations for the mode $n=0$ using Eq. (17). The dashed lines, showing the hybridized dispersion of the Damon-Eshbach mode and the first perpendicular standing spin-wave mode were calculated numerically for a continuous film with a thickness of 40 nm. On the right side the mode profiles are illustrated.

In order to understand the above experimental findings we need (i) to explain why every discrete mode is observed over a characteristic continuous range of transferred wave vectors, and (ii) to calculate the frequencies of the observed eigenmodes.

Since the discrete, dispersionless spin-wave modes ob-

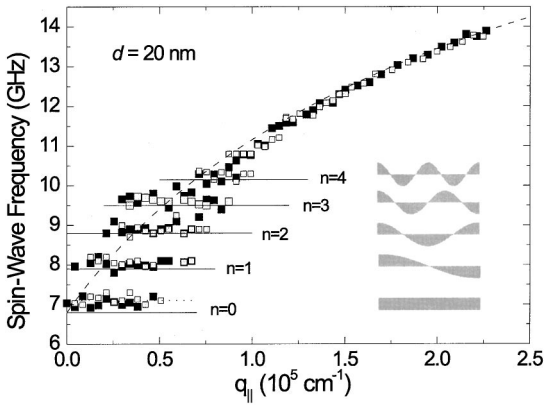

FIG. 5. Obtained spin-wave dispersion curves for an array of wires with a wire thickness of 20 nm, a wire width of 1.8 μm, and a separation between the wires of 0.7 μm (open symbols) and 2.2 μm (solid symbols). The external field applied along the wire's axis was 500 Oe. The solid horizontal lines indicate the results of a calculation using Eq. (7) with the quantized values of $q_{\parallel}$. The dotted horizontal line indicates the result of calculations for the mode $n=0$ using Eq. (17). The dashed line indicates the numerically calculated dispersion of a continuous film with a thickness of 20 nm. On the right side the mode profiles are illustrated.

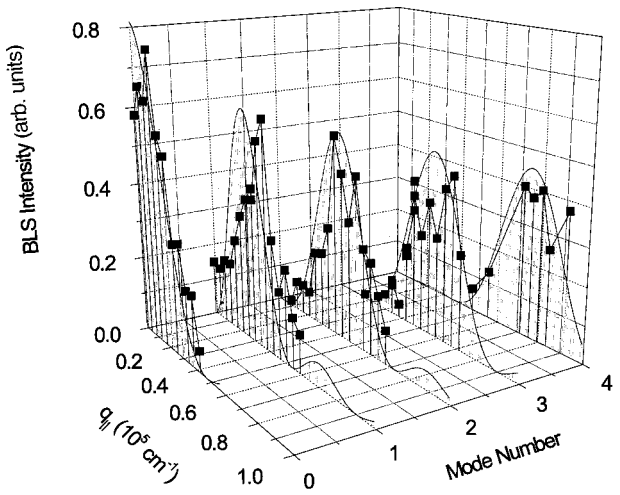

FIG. 6. Measured relative BLS intensities (black squares) of the in-plane quantized spin-wave modes as a function of the wave vector $q_{\parallel}$ and the mode number n in comparison to the calculated results based on Eq. (16) (gray colored curves).

served for small wave vectors converge towards the dispersion of the DE mode of the continuous film, it is natural to assume that these modes result from a width dependent quantization of the in-plane wave vector of the DE mode, discussed above. As it was shown, the profile of the dynamic part of the magnetization m in the nth mode has a cosinelike shape [see Eq. (11)]. On the other hand, the component of the transferred in-plane wave vector along the wire axis $q_{\parallel,z}$ is fully conserved in the light-scattering process. In our experiments $\mathbf{q}_{\parallel}$ was oriented perpendicular to the wires, $q_{\parallel,z}=0$. Therefore only the spin-wave modes with $q_z=0$, i.e., $m(z)=\text{const}$, can take part in the scattering process. This and the fact that $d \ll w$ justify to write Eq. (11) in a one-dimensional form, where m is considered to be a function of y only. In this case Eq. (15), which determines the light-scattering intensity $I(q)$, can be essentially simplified:

$$I(q) \propto \frac{d^2\sigma}{d\Omega\, d\omega_S} \propto \langle \delta\varepsilon^*(q)\, \delta\varepsilon(q) \rangle \propto |m_q|^2 = \left| \int_{-w/2}^{w/2} m(y) \cdot \exp(-iqy)\, dy \right|^2 . \quad (16)$$

Note here that since the integration is performed only within the wire, the Fourier transform m_q is nonzero over a continuous interval of q and thus the discrete modes are observed over a finite interval of the transferred wave vector $q_{\parallel}$. Substituting Eq. (11) in Eq. (16) and using Eq. (10), one can calculate the light-scattering intensity $I_n(q_{\parallel})$ for each standing lateral mode. The results of this calculation for the lowest five modes, normalized for the best fit of the $n=0$ mode, are shown in Fig. 6 by gray colored lines. A very good agreement between the experimental data and the results of the calculation justifies the chosen boundary condition and confirms that the observed spin-wave modes are in fact the quantized DE modes.

The frequency of the observed modes can be derived by substituting the obtained quantized values of wave vector $q_{y,n}$ into the dispersion equation of the DE mode, Eq. (7). The results of these calculations are shown in Figs. 4 and 5 by the solid horizontal lines. For the calculation the geometrical parameters (wire thickness $d=20$ or 40 nm, wire width $w=1.8\,\mu$m) and the independently measured material parameters $4\pi M_s=10.2$ kG and $\gamma/2\pi=2.95$ GHz/kOe were used. Without any fit parameters the calculation reproduces all mode frequencies with $n>0$ very well, and for the $n=0$ mode a reasonable agreement is achieved. Since the group velocity $V_g=2\pi\partial\nu/\partial q$ of the dipolar surface spin wave [cf. Eq. (7)] decreases with increasing wave vector, the frequency splitting of neighboring, width-dependent discrete spin-wave modes, which are equally spaced in q space ($q_{y,n}=n\pi/w$), becomes smaller with increasing wave vector $q_{y,n}$, until the mode separation is smaller than the frequency resolution in the BLS experiment and/or the natural linewidth, and the splitting is no longer observable in Figs. 4 and 5. The evolution of the mode frequencies with an increasing applied field, as illustrated in Fig. 3, can be described as well. The solid lines marked as ''Q-DE'' are calculated using Eq. (7) with the quantized values of wave vector. With the exception of the curve for $n=0$ they also demonstrate a very good agreement with the experiment.

Although the spatial distribution and the frequencies of the observed modes are well reproduced, the above approach ignores the correction of dynamic dipole fields due to the finite width of the wires. Since the magnetic dipole interaction is a long-range one, the strength of the field at a given position is determined not only by the amplitude of the dynamic magnetization in the vicinity of this position, but also by the spatial distribution of the dynamic magnetization far from this position. Therefore, due to finite-size effects caused by the side walls, the dipole fields accompanying a quantized mode in the wire differ from those of the DE mode of the infinite film with the same wave vector. This correction, which is small in any case for the wires with the high aspect ratio, is negligible for all modes with sufficiently high quantum numbers (i.e., for modes with either p or n larger than zero). It is, however, observable for the lowest, uniform mode ($p=0$, $n=0$). The finite-size effect can be easily taken into account for long wires with ellipsoidal cross section since the dynamic dipole field is homogeneous in this case. The corresponding frequency is given by the Kittel formula:[23]

$$\nu = \frac{\gamma}{2\pi} \cdot [(H + N_x \cdot 4\pi M_S) \cdot (H + N_y \cdot 4\pi M_s)]^{1/2}, \quad (17)$$

where N_x and N_y are the demagnetization factors along the x and y direction in the wire cross section (note here that the demagnetization factor along the wire N_z is negligible). In our particular case of a wire with a rectangular cross section, Eq. (17) is not exactly applicable, as the dynamic demagnetization field is not exactly homogeneous. However, since the thickness of the wire is much smaller than its width ($d \ll w$), one can consider this field to be approximately homogeneous in agreement with the analytical solution for demagnetizing fields of a rectangular prism found by Joseph and Schlömann.[24] The corresponding demagnetization factors are $N_y=2d/\pi w$, $N_x=1-N_y$. The calculated value of N_y is in a good agreement with that obtained from static measurements. The frequency of the lowest mode calculated on the basis of Eq. (17) using the above demagnetization factors is

shown by a dotted horizontal line in Figs. 4 and 5. Its field dependence is illustrated in Fig. 3 by a solid line, marked as ''Kittel.'' The agreement with the experiment is convincing. It is much more complicated to take into account the finite-size effects for the nonuniform modes. However, from the qualitative considerations it is obvious that the correction of the demagnetizing fields (or demagnetization factors) due to the finite size of the wire rapidly decreases with increasing mode number. Therefore good reproduction of the mode frequencies for $n>0$ just on the basis of Eq. (7) is not surprising.

As a final remark, let us emphasize the difference between the lateral spin-wave quantization observed in this work and the quantization of perpendicular standing spin waves in thin magnetic films. The former effect is the quantization of the dipole dominated spin waves with relatively small in-plane wave vectors and with frequencies determined by long-range interacting dipole fields, whereas the latter describes the spin waves with high wave vectors perpendicular to the film plane, defined by the thickness of the film and with frequencies determined by the exchange stiffness. Due to the long-range nature of the dipole fields, the laterally quantized spin waves can form collective excitations under appropriate conditions in arrays of wires. Investigations of such collective excitation are the subject of future studies.

In summary, we have observed spin-wave quantization in a periodic array of magnetic wires. The observed discrete modes can be understood as the width dependent quantization of the dipolar surface spin-wave mode (in-plane quantized DE mode). An excellent agreement between the calculated and measured values of (i) the frequency of the modes, (ii) the wave vector interval, where the modes are observed, and (iii) the BLS intensity versus wave vector dependence of each mode support our interpretation. For larger wave vectors quantized modes converge towards the dispersion of the infinite continuous film. No indication for zone-folding effects due to the periodicity of the wires was yet found.

ACKNOWLEDGMENTS

Support by the Deutsche Forschungsgemeinschaft, European Community network ''Dynaspin,'' and National Science Foundation (Grant No. DMR-9701640) is gratefully acknowledged.

[1] J. F. Smyth, S. Schultz, D. R. Fredkin, D. P. Kern, S. A. Rishton, H. Schmid, M. Cali, and T. R. Koehler, J. Appl. Phys. **69**, 5262 (1991).
[2] A. Maeda, M. Kume, T. Ogura, K. Kukori, T. Yamada, M. Nishikawa, and Y. Harada, J. Appl. Phys. **76**, 6667 (1994).
[3] N. Bardou, B. Bartenlian, F. Rousseaux, D. Decanini, F. Carcenac, E. Cambril, M.-F. Ravet, C. Chappert, P. Veillet, P. Beauvillain, R. Megy, W. Geerts, and J. Ferre, J. Magn. Magn. Mater. **148**, 293 (1995).
[4] A. O. Adeyeye, J. A. C. Bland, C. Daboo, J. Lee, U. Ebels, and H. Ahmed, J. Appl. Phys. **79**, 6120 (1996).
[5] C. Mathieu, C. Hartmann, M. Bauer, O. Buettner, S. Reidling, B. Roos, S. O. Demokritov, B. Hillebrands, B. Bartenlian, C. Chappert, D. Decanini, F. Rousseaux, E. Cambrill, A. Mueller, B. Hoffmann, and U. Hartmann, Appl. Phys. Lett. **70**, 2912 (1997).
[6] A. Ercole, A. O. Adeyeye, J. A. C. Bland, and D. G. Hasko, Phys. Rev. B **58**, 345 (1998).
[7] A. G. Gurevich and G. A. Melkov, *Magnetization Oscillations and Waves* (CRC Press, New York, 1996).
[8] B. A. Kalinikos and A. N. Slavin, J. Phys. C **19**, 7013 (1986).
[9] C. Herring and C. Kittel, Phys. Rev. **81**, 869 (1951).
[10] G. T. Rado and J. R. Weertman, J. Phys. Chem. Solids **11**, 315 (1959).
[11] R. W. Damon and J. R. Eshbach, J. Phys. Chem. Solids **19**, 308 (1961).
[12] B. Hillebrands, Phys. Rev. B **37**, 8885 (1988).
[13] R. E. DeWames and T. Wolfram, Appl. Phys. Lett. **16**, 305 (1970); J. Phys. (Paris) **32**, C1-1090 (1971).
[14] S. O. Demokritov and E. Tsymbal, J. Phys.: Condens. Matter **6**, 7145 (1994).
[15] B. Hillebrands, in *Light Scattering in Solids VII*, edited by G. Güntherodt and M. Cardona (Spinger, Heidelberg, in press).
[16] L. D. Landau and E. M. Lifshitz, *Electrodynamics of Continuous Media* (Pergamon Press, Oxford, 1960).
[17] M. G. Cottam and D. J. Lockwood, *Light Scattering in Magnetic Solids* (Wiley, New York, 1986).
[18] B. A. Gurney, P. Baumgart, V. Speriosu, R. Fontana, A. Patlac, T. Logan, and P. Humbert, in *Proceedings of the International Conference on Magnetic Films and Surfaces, Glasgow, 1991* (Institute of Physics, London, 1991), P7.12, p. 474.
[19] C. Mathieu, J. Jorzick, A. Frank, S. O. Demokritov, A. N. Slavin, B. Hillebrands, B. Bartenlian, C. Chappert, D. Decanini, F. Rousseaux, and E. Cambrill, Phys. Rev. Lett. **81**, 3968 (1998).
[20] F. Rousseaux, D. Decanini, F. Carcenac, E. Cambril, M. F. Ravet, C. Chappert, N. Bardou, B. Bartenlian, and P. Veillet, J. Vac. Sci. Technol. B **13**, 2787 (1995).
[21] R. Mock, B. Hillebrands, and J. R. Sandercock, J. Phys. E **20**, 656 (1987).
[22] B. Hillebrands, Rev. Sci. Instrum. **70**, 1589 (1999).
[23] C. Kittel, Phys. Rev. **73**, 155 (1948).
[24] R. I. Joseph and E. Schlömann, J. Appl. Phys. **36**, 1579 (1965).